EurJIC
European Journal of Inorganic Chemistry

A Journal of ChemPubSoc Europe

Accepted Article

Title: Tuning the Catalytic Activity of UiO-66 via Modulated Synthesis:Esterification of Levulinic Acid as A Test Reaction

Authors: Ruiping Wei, Jingdeng Fan, Xumin Qu, Lijing Gao, Yuanfeng Wu, Zhongqi Zhang, Feng Hu, and Guomin Xiao

To be cited as: *Eur. J. Inorg. Chem.* 10.1002/ejic.202000031

Link to VoR: http://dx.doi.org/10.1002/ejic.202000031

WILEY-VCH

WILEY-VCH

FULL PAPER

Tuning the Catalytic Activity of UiO-66 via Modulated Synthesis : Esterification of Levulinic Acid as A Test Reaction

Ruiping Wei*[a], Jingdeng Fan[a], Xumin Qu[a], Lijing Gao[a], Yuanfeng Wu[a], Zhongqi Zhang[a], Feng Hu[a], Guomin Xiao[a]

Abstract: Due to its high stabilities and tunable defects, Zirconium terephthalate UiO-66 type metal organic frameworks (MOFs) has been a promising catalyst in many catalytic reactions. The catalytic activity of UiO-66 MOFs is significantly affected by the density of defects and hydroxyl groups bonded to Zr_6 nodes, which can be tuned by modulators. In this work, a series of defective UiO-66 were synthesized via tuning the ratio of H_2BDC/Zr and adding monocarboxylic acids with different chain length as modulators. The synthesized UiO-66 MOFs were characterized by X-ray diffraction, N_2 physisorption, IR and ^{1}H NMR spectroscopies, scanning and transmission electron microscopy. Esterification of levulinic acid with ethanol was selected to reveal the influence of modulators, defects and hydroxyl groups. The results showed that UiO-66 with 0.5 of H_2BDC/Zr ratio and lauric acid as the modulator owned excellent catalytic activity. The cooperative effects, between the Lewis acid sites offered by unsaturated Zr_6 nodes and Brønsted acid sites supplied by OH, has been revealed to have a significant influence on the catalytic activity.

Introduction

Metal-organic frameworks (MOFs) are crystalline porous structures synthesized with organic linker molecules and inorganic metal clusters[1]. Due to their large internal surface areas and high degrees of defect tunability, MOFs have been widely investigated in separation[2], storage[3], sensor[4]. Notably, the high active site densities provided by unsaturated metal nodes, tailorable pore structures and ease of functionalization commend MOFs as a potentially materials in catalysis[5]. With incorporating Zr_6O_8 clusters as nodes, Zr-Based MOFs (UiO-66) has been one of the most promising and investigated MOFs as practical catalysts owing to its high stability under harsh conditions and appropriate acid sites by tuning structural defects[6].

Defective engineering in UiO-66 has drawn considerable attention because defects in structure could be exploited towards altering physical–chemical properties of the MOFs[7]. Ideal UiO-66, consisting of 12-coordinated hexanuclear $[Zr_6(\mu_3O)_4(\mu_3\text{-}OH)_4]^{12+}$ metal clusters connected to H_2BDC linkers, commonly has weak catalytic activity due to fewer Lewis acid sites provided by saturated Zr atom. In order to improve catalytic activity, defects were systematically introduced into UiO-66 via different methods including modulated synthesis. To form defect sites, HCl[8], TFA[9] or a monocarboxylic acid[10] is added to reaction solution as a modulator, which competes with H_2BDC linkers for bonding to the nodes to satisfy modulated synthesis. Whilst, the correlation between catalytic activities and defects has been studied by many researchers. Ma et al.[11] systematically investigated the influence of structural defects in Pt@UiO-66-NH_2 on photocatalytic properties and proved that structural defects could switch on photocatalysis. Vermoortele et al.[12] synthesized defective UiO-66 with trifluoroacetic acid and HCl as modulators, and further probed the relationship between catalytic activity and numbers of defect in cyclization of citronellal. Liu et al.[13] quantified the numbers of defects by a potentiometric acid-base titrations and established the quantitative correlations between defects and catalytic activity by an epoxide ring-opening reaction. Catalytic activity is not only affected by defects such as missing linkers and nodes, but also related to structure and properties of ligands bonded to Zr_6O_8 in UiO-66. Recently, the hydroxyl groups on nodes as Brønsted acid sites were evaluated by some reports[14]. Klet et al.[15] considered that the hydroxyl groups on Zr_6O_8 are μ_3-OH, Zr-OH_2 and Zr-OH. And their Brønsted acidity values were evaluated quantitatively by Potentiometric acid–base titration. Yang et al.[16] determined the ligands on the node surfaces by IR and ^{1}H NMR and used ethanol dehydration to probe the correlation between the ligands on the Zr_6O_8 surfaces and catalytic properties.

Our previous work[17] has investigated the effects of node groups on the properties of Zr_6O_8 and presented that the properties of ligands could be indicated by μ_3-OH. To our best knowledge, tuning systematically the numbers of defect sites and the hydroxyl groups on Zr_6O_8 in defective UiO-66 with long chain monocarboxylic acids was yet to be explored. Due to efforts have been devoted to reveal the effects of ligands and groups on the Zr_6O_8 node, catalytic activity has not been focused on, especially about the hydroxyl groups. Therefore, in this work, a series of defective UiO-66 were synthesized by adjusting the ratio of H_2BDC/Zr and adding monocarboxylic acids with different chain length as a modulator. Esterification of levulinic acid with ethanol, which is mainly dominated by Brønsted acid sites was chosen as a test reaction to well understand the correlation between defects and properties of ligands on Zr_6O_8 provided by the hydroxyl groups such as μ_3-OH on Zr_6O_8 nodes (**Figure 1**).

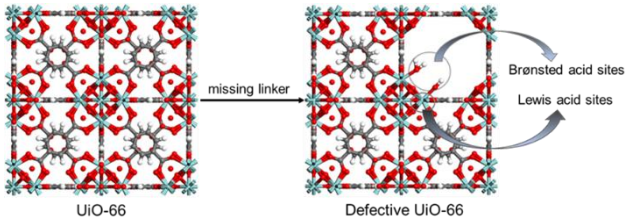

Figure 1. Schematic representation of UiO-66 and defective UiO-66

[a] Prof. R. Wei, M. J. Fan, M. X. Qu, Prof. L. Gao, Dr. Y. Wu, Dr. Z. Zhang, M. F. Hu, Prof. G. Xiao
School of Chemistry and Chemical Engineering
Southeast University, Nanjing, Jiangsu, China
E-mail: weiruip@seu.edu.cn
http://publons.com/researcher/3364312/ruiping-wei/

Results and Discussion

Properties of UiO-66 with different precursor ratios

The effects of H_2BDC/Zr on the crystallinity and structural purity of as-prepared materials were analyzed by XRD (**Figure 2**). The characteristic diffraction peaks of all synthesized UiO-66 MOFs were consistent with previous report[18], attributing to the (111) reflection (2θ=7.3°), (002) reflection (2θ=8.5°) and (115) reflection (2θ=25.7°) and proving the successful preparation of UiO-66 modulated synthesis. As shown in **Figure 2**, the intensity of characteristic peaks of UiO-66 increased slightly with the ratio of H_2BDC/Zr from 0.3 to 1.0, and maintained certain intensity with increasing the ratio of H_2BDC/Zr from 1.0 to 2.0. The results showed that the crystallinity of samples was affected by the ratio of H_2BDC/Zr to some extent.

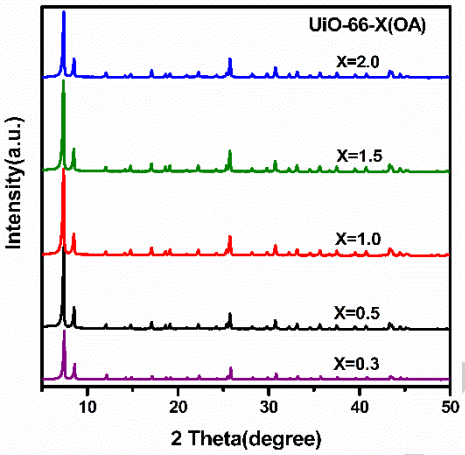

Figure 2. XRD patterns of UiO-66-X(OA)

The porosities and surface area of UiO-66 MOFs via modulated synthesis with different mole ratio of H_2BDC/Zr were analyzed by N_2 adsorption–desorption isotherms. The influence of precursor ratios was clearly reflected in **Figure 3**. The obviously increase of adsorption amount under relative pressure (P/P_0) less than 0.1 revealed the pores were mainly microporous. Meanwhile, there was a tendency that the volume adsorbed increased from 400 $cm^3 \cdot g^{-1}$ to 590 $cm^3 \cdot g^{-1}$ with the decrease of the ratio of H_2BDC/Zr when the ratio was more than 0.5. With a further decrease of the ratio to 0.3, the N_2 adsorption amount of UiO-66 decreased to 510 $cm^3 \cdot g^{-1}$ from 590 $cm^3 \cdot g^{-1}$. In addition, an obvious hysteresis loop was found in the N_2 adsorption–desorption isotherms of UiO-66-0.5(OA), which indicated the existence of mesopores in the material.

To further compare the BET surface area and characteristics of porosity of materials synthesized under different ratios, specific data of them were listed in **Table 1**. The overall trend in BET area and porosity features was consistent with that of the N_2 adsorption amount of the synthesized UiO-66 samples. From the data in **Table 1**, the conclusion could be drawn more intuitively that the pores of materials were mainly microporous and partly mesoporous. It was worth noting that the BET surface area and pore volume of UiO-66-0.5(OA) were up to 1266 $cm^2 \cdot g^{-1}$ and 0.93 $cm^3 \cdot g^{-1}$, respectively. Moreover, the largest mesopore volume was obtained in UiO-66-0.5(OA) sample compared to other synthesized ones explained the existence of hysteresis loop in the N_2 adsorption–desorption isotherms of UiO-66-0.5(OA). The differences in BET area and porosity features of UiO-66 might be attributed to the number of missing-node defects and missing-linker defects, which were tuned by the ratio of precursor. In other words, the reduced amount of H_2BDC meant that more modulators pre-occupied the coordination sites could be retained but not replaced by linker, leading to larger pore volume and surface area of the prepared materials. Nevertheless, excessively insufficient H_2BDC was also be detrimental to the formation of defects and mesoporous structures owing to the coordination between Zr-oxo clusters and H_2BDC was hampered by an excess of modulators.

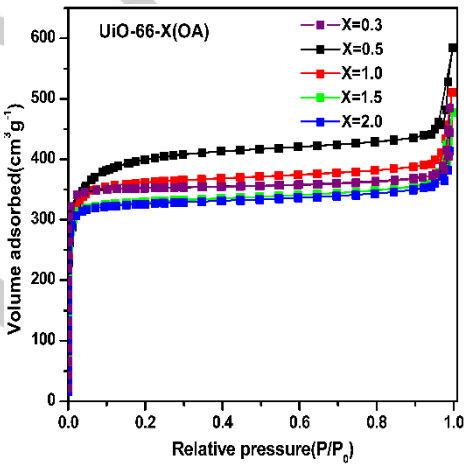

Figure 3. N_2 adsorption–desorption isotherms of UiO-66-X(OA)

Table 1 Surface area and pore structure of UiO-66-X(OA)

Sample	S_{BET} (m^2/g)	S_{Micro} (m^2/g)	S_{Meso} (m^2/g)	V_{Total} (cm^3/g)	V_{Micro} (cm^3/g)	V_{Meso} (cm^3/g)
X=0.3	960	940	20	0.61	0.48	0.13
X=0.5	1266	1181	85	0.93	0.61	0.32
X=1.0	1113	1049	64	0.79	0.55	0.24
X=1.5	1013	946	67	0.74	0.51	0.23
X=2.0	988	938	50	0.64	0.50	0.14

The morphology of UiO-66 samples was measured by SEM. **Figure 4** showed the differences in cubic morphology and particle size of UiO-66 synthesized with various ratios of H_2BDC/Zr. The evident typical octahedral cubic crystal was observed in **Figure 4c**, which indicated that the relative crystallinity of the material was much high when the ratio of H_2BDC/Zr was 1.0. However, the octahedral cubic morphology was gradually transformed into spheroid, whether increasing or decreasing the ratio of H_2BDC/Zr. The result revealed that the morphology and crystallinity of UiO-66 samples could be tuned by altering the ratio of H_2BDC/Zr, which was consistent with the result of XRD patterns. Similarly,

the particle size of UiO-66 materials was regulated via changing the precursor ratio. When the ratio of H_2BDC/Zr was less than 1.0, the average particle size of the UiO-66 samples increased with the increase of the ratio of H_2BDC/Zr. However, when the ratio of H_2BDC/Zr was more than 1.0, an obvious decrease in the average particle size of the UiO-66 could be seen with increasing the ratio of H_2BDC/Zr. Besides, the UiO-66 samples with uniform size and narrow size distribution could be obtained with tuning the ratio of H_2BDC/Zr to 0.5.

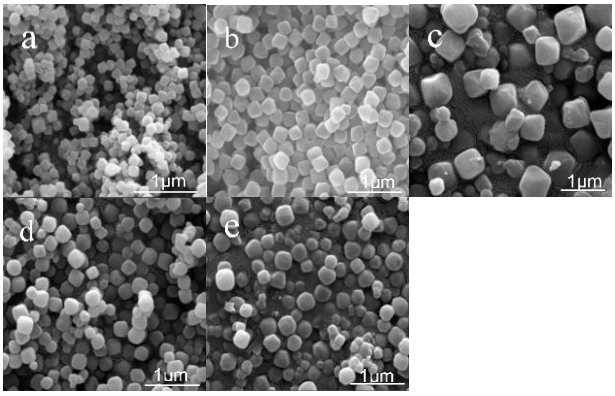

Figure 4. SEM of UiO-66-X(OA) (a) X=0.3, (b) X=0.5, (c) X=1.0, (d) X=1.5 and (e) X=2.0

The data of defect site density per node on UiO-66 were estimated by liquid ^{1}H NMR spectra, which could determine accurately the relative concentrations of the molecular components bonded per node[16,17]. As shown in **Table 2**, the overall trend of data were consistent with that of BET surface area and pore volume. The number of defects in UiO-66 increased first and then decreased with increasing the ratio of H_2BDC to Zr. The number of defects on the MOFs nodes could be up to 1.61 by tuning the ratio of H_2BDC/Zr to 0.5.

Table 2 Influence of ratio of H_2BDC/Zr on the number of defects per node determined from ^{1}H NMR spectra

UiO-66-X(OA)	number of formate ligands	number of DMF ligands	number of octanoate ligands	number of defects
X=0.3	0.28	0.26	0.25	0.79
X=0.5	0.17	0.19	1.25	1.61
X=1.0	0.62	0.58	0.29	1.49
X=1.5	0.42	0.43	0.06	0.91
X=2.0	0.28	0.29	0.09	0.66

Figure 5 showed the correclation between ratio of H_2BDC/Zr, number of defects and the catalytic activity of UiO-66 in the esterification of levulinic acid with ethanol. In all cases ethyl levulinate (EL) selectivity was 100 %. There was an obvious correlation between yield of EL and ratio of H_2BDC/Zr. The yield of EL was improved from 40% to 77% with the increase of ratio of H_2BDC/Zr from 0.3 to 0.5. However, the yield of EL decreased gradually to 40% when the ratio was further increased to 2.0. In short, the preferential order to EL was found to be: UiO-66-0.5(OA) > UiO-66-1.0(OA) > UiO-66-1.5(OA) > UiO-66-2.0(OA) > UiO-66-0.3(OA). That meaned the highest EL yield (77%) was achieved via tuning the ratio of H_2BDC/Zr to 0.5 under constant catalytic conditions. The variation trend of catalytic activity was coincided with that of surface area, pore volume and number of defects. Based on the characterization of materials, especially the analysis of BET and H^1NMR, it was not difficult to explain the catalytic result. The observed high activity of UiO-66-0.5(OA) was probably ascribed to large surface area and uniform crystal size providing the probability of contact between the reactant and active sites, and enough pore volume promoting the transfer of products from active sites. Moreover, the more defects in structure provided more active sites conducive to the esterification of levulinic acid with ethanol. The interaction of several factors endowed the UiO-66-0.5(OA) samples excellent catalytic activity.

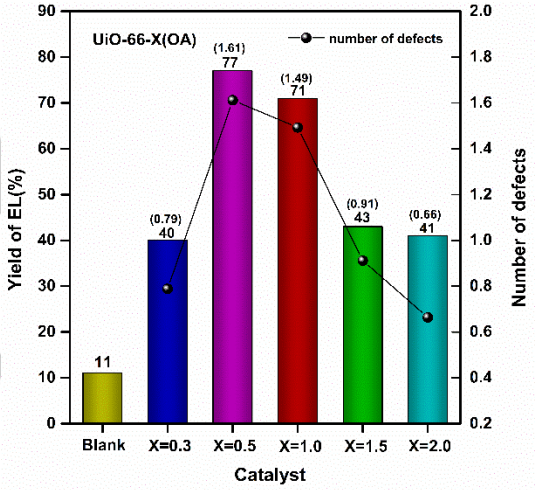

Figure 5. The correclation between ratio of H_2BDC/Zr, number of defects and yield of EL

Properties of UiO-66 with different modulators

In addition to changing the precursor ratio, many reports confirmed that monocarboxylic acid could be introduced into system to tune defect site density and thus bring out high activity[7a, 12, 19]. Therefore, the influence of chain length in modulators on properties of UiO-66 was further investigated with the precursor ratio constant at 0.5 of H_2BDC/Zr, an optimal one for synthesis of UiO-66 MOFs.

Figure 6 exhibited the crystallinity of sysnthesed materials using monocarboxylic acids with different chain length as modulators. The intensity of main diffraction peaks of samples using acetic acid and octanoic acid with shorter chain length as modulators were relatively high. Further extending the length of the alkyl chain, a significant decrease in intensity of peaks was observed. Notably, a peak broadening was seen in the XRD spectrum of UiO-66 with myristic acid as a modulator, which clearly revealed that the

formation of UiO-66 could be disturbed if monocarboxylic acids with too long chain as modulators. The main reason for the result was that the extended chain of the modulator blocked the coordination between Zr^{IV} and H_2BDC[20].

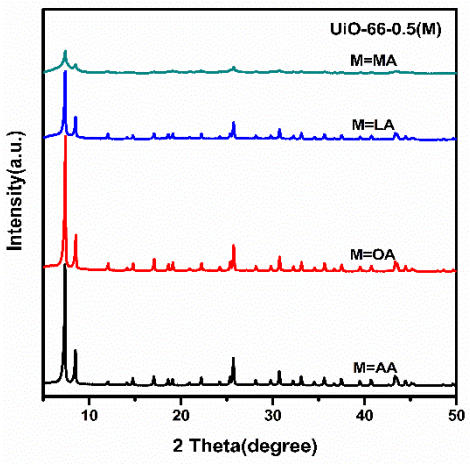

Figure 6. XRD patterns of UiO-66-0.5(M)

Figure 7 showed the N_2 adsorption–desorption isotherms of samples synthesized with different monocarboxylic acids as modulators respectively. When the ratio of H_2BDC/Zr was determined, the adsorbed quantity of UiO-66 samples depended mainly on the alkyl chain length of monocarboxylic acids. As the number of carbon atoms of the alkyl chain increased from 2 to 12, the amount of N_2 adsorption over the synthesized UiO-66 samples was up to 800 $cm^3 \cdot g^{-1}$. Unexpectedly, further increasing the chain length of modulators, the N_2 adsorption amount of the UiO-66 decreased dramatically from 800 $cm^3 \cdot g^{-1}$ to 400 $cm^3 \cdot g^{-1}$. Meanwhile, a small hysteresis loop was observed in the N_2 adsorption–desorption isotherms of UiO-66-0.5(AA) and UiO-66-0.5(OA). Further increasing the chain length, a more pronounced hysteresis loop was found in UiO-66-0.5(LA), which indictatd the long length modulators were crucial in the formation of mesoporous.

Table 3 Surface area and pore structure of UiO-66-0.5(M)

Sample	S_{BET} (m^2/g)	S_{Micro} (m^2/g)	S_{Meso} (m^2/g)	V_{Total} (cm^3/g)	V_{Micro} (cm^3/g)	V_{Meso} (cm^3/g)
M=AA	1148	1102	46	0.84	0.59	0.25
M=OA	1266	1181	85	0.93	0.61	0.32
M=LA	1409	1314	95	1.25	0.69	0.56
Used (LA)	1000	912	88	1.01	0.49	0.52
M=MA	346	259	87	0.63	0.17	0.46

The surface area and pore volume of samples with different modulators were listed in **Table 3**. The moderate elongation of alkyl chain increased significantly the surface area and porous volume. The surface area and pore volume of UiO-66-0.5(LA) were up to 1409 $cm^2 \cdot g^{-1}$ and 1.23 $cm^3 \cdot g^{-1}$ respectively. In addition, the mesoporous volume in UiO-66-0.5(OA) was also the largest compared to that in samples synthesized with other modulators. When myristic acid was used a modulator, the surface area of UiO-66 decreased to 346 $cm^2 \cdot g^{-1}$ from 1409 $cm^2 \cdot g^{-1}$ and the pore volume decreased to 0.63 $cm^3 \cdot g^{-1}$ from 1.25 $cm^3 \cdot g^{-1}$, due to collapse of structure.

Combined with the analysis results of XRD and BET, we found that moderate chain length in modulators could increase the adsorption amount, surface area and pore volume while ensure the crystallinity of UiO-66 materials. Nevertheless, excessively long alkyl chain disturbed the formation of UiO-66, thus leading to the decreases of surface area and pore volume

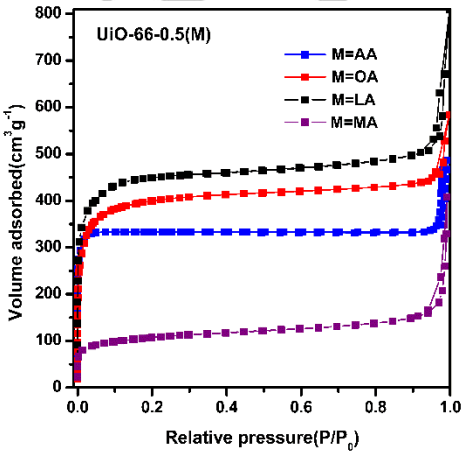

Figure 7. N_2 adsorption–desorption isotherms of UiO-66-0.5(M)

The length of alkyl chain in modulators clearly affected the morphology and the particle size of UiO-66, which was confirmed by the SEM (**Figure 8**). As shown in **Figure 8a**, the octahedral cubic structure was possessed by the UiO-66 with acetic acid as a modulator and the average particle size was about 350 nm. With the increase of alkyl chain length from 2 to 12 carbon atoms, the octahedral cubic morphology was gradually transformed into smooth spheroid and the particle size decreased from 350 nm to 220 nm. However, there were existences of the particle aggregation and the collapse of crystal morphology in **Figure 8d**, the SEM of UiO-66-0.5(MA) synthesized with myristic acid (14 atoms in the alkyl chain) as a modulator. Combined with SEM and XRD results, a conclusion could be deduced that the number of carbon atoms in the alkyl chain of modulators was about 12 at most, to ensure the morphology and crystallinity.

To further reveal the influence of the alkyl chain length in modulators on micropore and mesopore structure, UiO-66-0.5(M) (M=AA, OA and LA) with high relative crystallinity were chosen to measure by TEM. Compared with SEM, the TEM showed more clearly the transformation of crystalline structures in UiO-66 materials with the elongation of alkyl chain in modulators. There was no obvious structure of mesopore observed in the UiO-66-0.5(AA) sample (**Figure 9d**). Instead, the worm-like mesopores were found in the UiO-66-0.5(OA) (**Figure 9e**) and UiO-66-0.5(LA) (**Figure 9f**), which demonstrated that the formation of

mesopores could be tuned by suitable alkyl chain length of modulators. The result was in accordance with **Table 3** and further indicated the defects and pore structure could be also controlled by the modulators with different alkyl chain length.

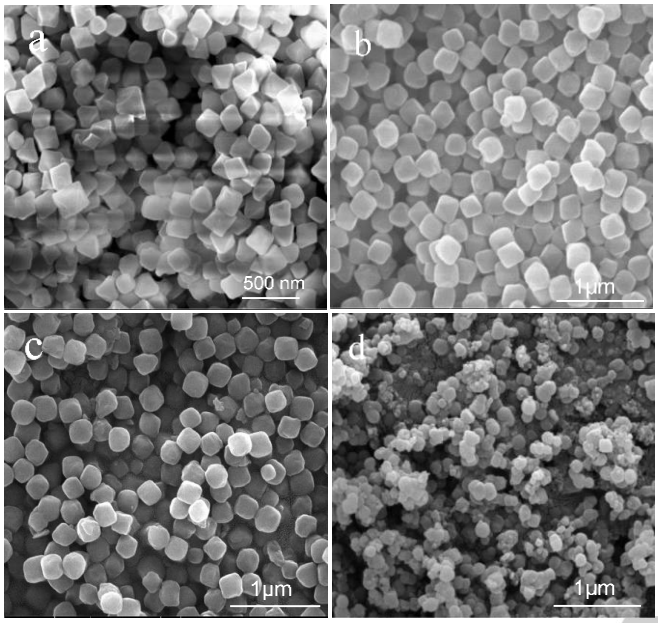

Figure 8. SEM of UiO-66-0.5(M) (a) M=AA, (b) M=OA, (c) M=LA, and (d) M=MA

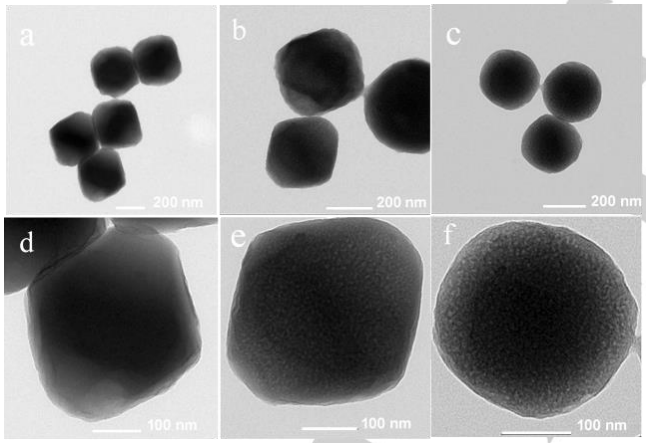

Figure 9. TEM of UiO-66-0.5(M) (a,d) M=AA, (b,e) M=OA and (c,f) M=LA

IR spectra could identify the hydroxyl groups incorporated on Zr_6 nodes[14b, 17, 21], which acted as Brønsted acid sites in catalytic reactions. Therefore, we studied the influence of different modulators on proton topology of Zr_6 node vacancies in UiO-66 samples by IR, which was shown in **Figure 10a**. The peak observed at 3671 cm^{-1}, 3670 cm^{-1} and 3667 cm^{-1} possessed by the UiO-66 were assigned to the μ_3-OH stretching frequency bonded to Zr_6 nodes[17, 22]. The μ_3-OH band shifted slightly to low frequencies at 3667 cm^{-1} from 3671 cm^{-1} when lauric acid with long alkyl chain was used as a modulator. The reason for the red shift of μ_3-OH stretching frequencies should be that the number of vacancies on per Zr_6 node increased with extending the alkyl chain length of modulators[16]. To further explain why catalytic activity of activated UiO-66 catalysts reduced compared to UiO-66 without activation, the change of hydroxyl groups bonded to nodes between UiO-66-0.5(LA) and UiO-66-0.5(LA) activated at 353 k for 12 h under vacuum was investigated (**Figure 10b**). The OH stretching region almost disappeared after activation, which confirmed that the IR band at 3647 cm^{-1}, 3647 cm^{-1} and 3633 cm^{-1} in UiO-66-0.5(AA), UiO-66-0.5(OA) and UiO-66-0.5(LA) respectively were assigned to a new OH stretching introduced by H_2O capping the vacant site. The result was consistent with previous report[22].

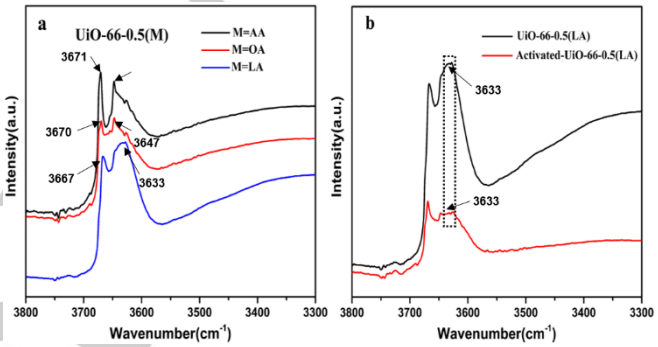

Figure 10. IR spectra in v_{OH} region characterizing (a) UiO-66-0.5(M); (b) UiO-66-0.5(LA) and the same sample activated at 353 k for 12 h under vacuum

The data in **Table 4** were estimated by liquid ^{1}H NMR spectra, which could unravel the effects of modulators in the MOF synthese. **Table 4** showed that the variation of the alkyl chain length of the modulator in the synthesis allowed the tuning of the defect numbers. As shown in **Table 4**, the number of ligands derived from modulator were the main contributors to more defects on the MOF nodes. The number of defects per node in UiO-66-0.5(LA) could be up to 2.1, a relatively high defect site density. The defect site density was also affected by the pK_a of modulators. Generally, more defects would be formed with increase of acidity of modulators[16]. But, maybe the effect of the chain length on the defects was greater than that of the acid strength in present case, which promoted more defects generated in UiO-66-0.5(OA).

Table 4 Influence of modulator on the number of defects per node determined from ^{1}H NMR spectra

UiO-66-0.5(M)	number of formate ligands	number of DMF ligands	number of acetate, octanoate or laurate ligands	number of defects
M=AA	0.27	0.28	0.77(acetate)	1.32
M=OA	0.17	0.19	1.25(octanoate)	1.61
M=LA	0.21	0.20	1.69(laurate)	2.10
Activated(LA)	0.26	0.27	1.01((laurate))	1.54

The correclation between modulators, number of defects and catalytic activity of UiO-66 was further evaluated under same reaction conditions (**Figure 11**). To confirm the role of synthesized UiO-66 on the esterification of levulinic acid with ethanol, the blank reaction was conducted as a supplementary experiment, the EL yield of which was only 11% (**Figure 11**). The catalytic activity increased initially and then decreased with the elongation of alkyl chain in modulators. The yield of EL could reach 84% over the UiO-66 catalysts with lauric acid as a modulator. The yield of EL decreased from 84% to 33% when UiO-66-0.5(MA) was used as catalyst, because the excessively long alkyl chain in modulators disturbed the structure and decreased sharply the surface area and pore volume of UiO-66, which was confirmed by XRD, SEM and BET. The increased activity was primarily attributed to the excellent properties that UiO-66-0.5(LA) possessed. The UiO-66-0.5(LA) catalyst with high surface area could offer enough acid sites to activate reagent molecules and promote the reactivity. In addition, the more mesoporous inside UiO-66-0.5(LA) benefited the inner diffusion of bulkier reactant molecules and thus improved the catalytic activity. Meanwhile, the defects in UiO-66-0.5(LA) acted as Lewis acid sites was a factor to bring out high activity. The influence of hydroxyl groups on Zr_6 nodes on catalytic activity of UiO-66 was also studied. Compared with UiO-66-0.5(LA), the activity of activated UiO-66-0.5(LA) material decreased as a result of the decrease in number of defects and the almost disappearance of hydroxyl group. Generally, higher catalytic activity could be obtained with more defects in UiO-66 catalysts. However, though the number of defects in activated UiO-66-0.5(LA) was more than that in UiO-66-0.5(AA), the yield of EL with AA-0.5 as a catalyst was higher than that with UiO-66-0.5(LA) as a catalyst, which indicated that -OH and μ_3-OH on Zr_6 nodes acted as Brønsted acid sites was a crucial factor in the esterification of levulinic acid with ethanol.

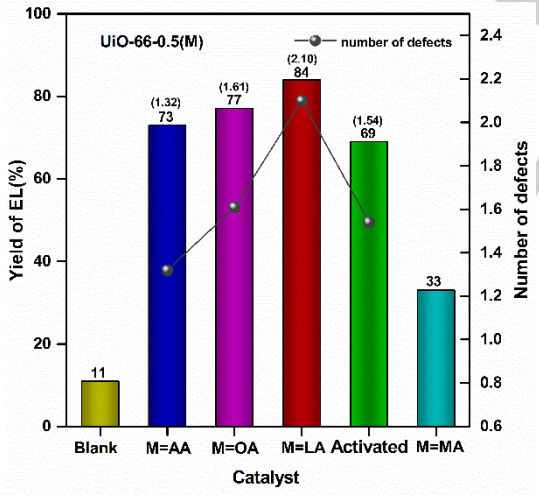

Figure 11. The correclation between modulators, number of defects and yield of EL

The reusability of UiO-66-0.5(LA) catalyst was studied in esterification of levulinic acid with ethanol under same experimental conditions of reaction temperature of 351 K, LA to ethanol molar ratio of 1:15 and reaction time of 8 h. After the reaction, the catalyst was recovered by centrifugation, washing with methanol, and then drying at room temperature overnight. The obtained results from recycling experiments were shown in **Figure 12**. No significant decrease of catalytic activity was seen, which signified that the synthesized catalyst possessed excellent reusability under this reaction conditions.

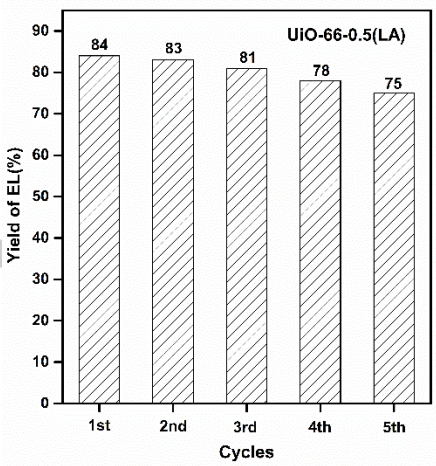

Figure 12. Reusability of UiO-66-0.5(LA) catalyst

To further check the stability of UiO-66-0.5(LA) catalyst, the used sample was characterized by XRD (**Figure 13**) and N_2 physisorption (**Figure 14**). No noticeable change in crystal structure was observed for the used catalyst, demonstrating that UiO-66-0.5(LA) had long-term stability. As seen in **Figure 13** and **Table 3**, compared to fresh sample, the surface area of the used UiO-66-0.5(LA) decreased to 1000 $cm^2 \cdot g^{-1}$ from 1409 $cm^2 \cdot g^{-1}$ and the pore volume the used UiO-66-0.5(LA) decreased to 1.01 $cm^3 \cdot g^{-1}$ from 1.25 $cm^3 \cdot g^{-1}$, hence leading to the slight decrease in catalytic activiity.

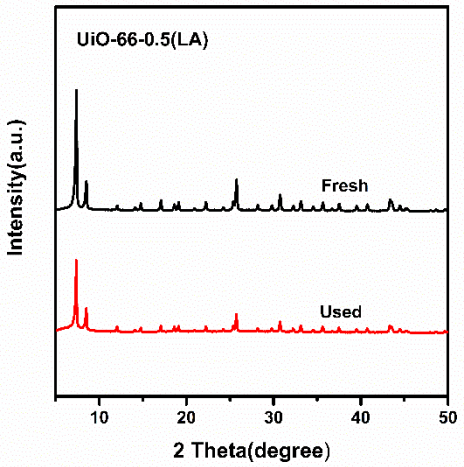

Figure 13. XRD patterns of fresh UiO-66-0.5(LA) and used UiO-66-0.5(LA) after five times

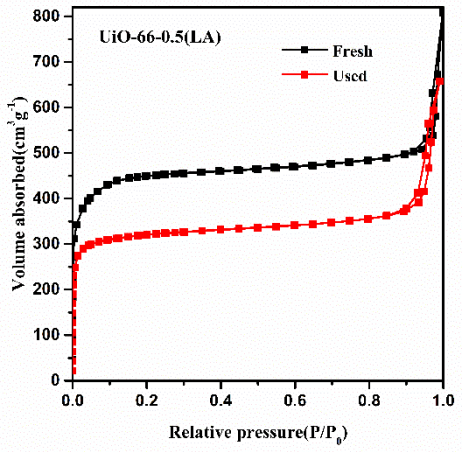

Figure 14. N_2 adsorption–desorption isotherms of fresh UiO-66-0.5(LA) and used UiO-66-0.5(LA) after five times

Conclusions

A series of defective UiO-66 with different defect densities were successfully synthesized by tuning the ratio of H_2BDC/Zr and adding monocarboxylic acids with different chain length as modulators. The UiO-66 MOFs synthesized with 0.5 of H_2BDC/Zr possessed higher surface area, pore volume, uniform particle size and higher defect density than that synthesized with other ratios. Meanwhile, the number of carbon atoms in modulator was 12 at most for ensuring the crystallinity and structure. Thus, the most active UiO-66 was synthesized with largest surface area, pore volume, uniform particle size and the highest defect density (2.1 per cluster) when the ratio of H_2BDC/Zr was 1:0.5 and Lauric acid was used as a modulator. In addition, the comparative experiment between UiO-66-0.5(LA) and activated UiO-66-0.5(LA) confirmed that the μ_3-OH and OH introduced by H_2O acted as Brønsted acid sites in catalytic reactions. The yield of EL was up to 84% at 351 K for 8 h catalyzed by the cooperative effect between Lewis acid sites and Brønsted acid sites. In addition, the synthesized defective UiO-66 also had excellent stability. This research provided a strategy to facilely tune the defect density and hydroxyl groups on nodes by introducing monocarboxylic with optimum alkyl chain length. The confirmation of cooperative effect between defects and hydroxyl groups can be considered when designing active UiO-66 for Brønsted acid catalyzed reactions.

Experimental Section

Materials

$ZrCl_4$ (99.9%) and levulinic acid (99%) were purchased from Aladdin. Ethanol (99.9%), Methanol (99%), acetic acid (AA, 99%), octanoic acid (OA, 99%), lauric acid (LA, 98%), myristic acid (MA, 98%), D_2O (99%), NaOH (96%) and DMF (99.5%) were purchased from Sinopharm Chemical Regent co. Ltd. All reagents were used without further purification.

Synthesis

synthesis of UiO-66 with different precursor ratios. $ZrCl_4$ (360 mg,1.55 mmol) and 8.7 ml octanoic acid (54.25 mmol, 35 equivalents with respect to Zr^{4+}) were dissolved in 60 ml DMF in a 100 ml Teflon liner with ultrasound for five minutes at room temperature. After that, different amounts of terephthalic acid (77 mg, 129 mg, 258 mg, 387 mg, and 516 mg, about 0.3, 0.5, 1.0, 1.5 and 2.0 equivalents with respect to Zr^{4+} respectively) were separately added into the mixed solution and dissolved for 15 minutes with ultrasound. The resulting solution was then transferred into a preheated oven at 393 K for 48 h without stirring. After centrifugation, the white crystalline powders were washed with fresh DMF two times to remove unreacted precursors and soaked in methanol 24 h (centrifugation every 8 h). After dried at room temperature, the resulting catalysts were denoted as UiO-66-X(OA), where X stands for the mole ratio of H_2BDC and Zr.

Synthesis of UiO-66 with different Modulators. $ZrCl_4$ (360 mg,1.55 mmol) and 54.25 mmol different monocarboxylic acids (acetic acid, octanoic acid, lauric acid and myristic acid, 35 equivalents with respect to Zr^{4+}) were dissolved in 60 ml DMF in a 100 ml Teflon liner with ultrasound for five minutes at room temperature. Terephthalic acid (linker, 129 mg, 0.775 mmol) was added into the above mixed solution and dissolved for 15 minutes with ultrasound. The resulting solution was then transferred into a preheated oven at 393 K for 48 h without stirring. After centrifugation, the white crystalline powders were washed with fresh DMF two times to remove unreacted precursors and soaked in methanol 24 h (centrifugation every 8 h). After dried at room temperature, the resulting catalysts were denoted as UiO-66-0.5(M), where M stands for the modulator (AA, OA, LA and MA).

Characterization

Powder X-ray Diffraction. Power X-ray diffraction (PXRD) patterns of UiO-66 were obtained using a Rigaku D/max-A diffractometer. The scanning range (2θ) was 5–50°, with a scanning rate of 10°·min^{-1} and a step function of 0.02°.

BET Surface Area Measurements. All N_2 adsorption–desorption isotherms were collected with a Beishide 3H-2000 analyzer by static N_2 physisorption at 77 K after samples were degassed at 393 K for 12 h under vacuum. The surface area of the UiO-66 was calculated based on multipoint Brunauer–Emmett–Teller (BET) method.

^{1}H NMR Spectroscopy. Liquid ^{1}H NMR spectra were recorded with a Bruker Avance DPX-500 NMR spectrometer (500 MHz). Samples were prepared by adding 15 mg UiO-66 into a 2 ml vial with 1 ml solution consisting of 1 M NaOH in D_2O, which could only dissolved the organic portion of the MOF (linker, solvent, components formed from the modulator, and any other such components)[16,17]. After digesting 24 h, the clear solution was transferred into an NMR tube.

Infrared Spectroscopy. The transmission IR spectra of MOF powder samples was collected by a Bruker IFS 66v/S spectrometer with a spectral resolution of 2 cm^{-1}.

Scanning Electron Microscopy. After the gold sputtering treated three times, the morphology of UiO-66 samples was measured by a FEI Inspect F50 SEM instrument.

Transmission Electron Microscopy. The samples measured were dispersed in Ethanol by ultrasound for 30 minutes. Then,

TEM images were collected with a FEI Tecnai G2 T20 TEM instrument.

Catalytic Test

Esterification of levulinic acid with ethanol was carried out in a bath reactor with 1:15 of molar ratio (levulinic acid: ethanol), 1.8 mol% of catalyst amount with respect to levulinic acid, 351 K of reaction temperature and 8 h of reaction time. The reaction products were analyzed by gas chromatography (GC-6890) equipped with SE-54 capillary column (30 m×0.32 mm×0.3 μm) and an FID detector. Analysis conditions were as follows: 443 K of column oven temperature, 543 K of injector temperature, and 553 K of detector temperature. Octane was used as the internal standard.

Acknowledgements

This work was financially supported by Natural Science Foundation of Jiangsu Province (No. BK20161415), National Natural Science Foundation of China (No. 21676054), Fundamental Research Funds for the Central Universities (No. 3207049413).

Keywords: Metal−organic framework • UiO-66 • Modulators • Defects • Levulinic acid

[1] a) S. Yuan, L. Feng, K. C. Wang, J. D. Pang, M. Bosch, C. Lollar, Y. J. Sun, J. S. Qin, X. Y. Yang, P. Zhang, Q. Wang, L. F. Zou, Y. M. Zhang, L. L. Zhang, Y. Fang, J. L. Li, H. C. Zhou, *Adv. Mater*. **2018**, *30*, 1704303; b) H. Furukawa, K. E. Cordova, M. O'Keeffe, O. M. Yaghi, *Science* **2013**, *341*, 1230444; c) M. T. Zhao, Y. Huang, Y. W. Peng, Z. Q. Huang, Q. L. Ma, H. Zhang, *Chem. Soc. Rev*. **2018**, *47*, 6267-6295; d) Z. Yin, S. Wan, J. Yang, M. Kurmoo, M. H. Zeng, *Coord. Chem. Rev*. **2019**, *378*, 500-512.

[2] a) S. L. Qiu, M. Xue, G. S. Zhu, *Chem. Soc. Rev.* **2014**, *43*, 6116-6140; b) J. R. Li, J. Sculley, H. C. Zhou, *Chem. Rev*. **2012**, *112*, 869-932.

[3] a) L. Wang, Y. Z. Han, X. Feng, J. W. Zhou, P. F. Qi, B. Wang, *Coord. Chem. Rev.* **2016**, *307*, 361-381; b) D. X. Xue, Q. Wang, J. F. Bai, *Coord. Chem. Rev.* **2019**, *378*, 2-16.

[4] a) Z. C. Hu, B. J. Deibert, J. Li, *Chem. Soc. Rev*. **2014**, 43, 5815-5840; b) Z. Z. Lu, R. Zhang, Y. Z. Li, Z. J. Guo, H. G. Zheng, *J. Am. Chem. Soc*. **2011**, *133*, 4172-4174.

[5] a) J. Lee, O. K. Farha, J. Roberts, K. A. Scheidt, S. T. Nguyen, J. T. Hupp, *Chem. Soc. Rev.* **2009**, *38*, 1450-1459; b) J. D. Xiao, H. L. Jiang, *Accounts Chem. Res.* **2019**, *52*, 356-366; c) K. Chen, C. D. Wu, *Coord. Chem. Rev.* **2019**, *378*, 445-465; d) Y. B. Huang, J. Liang, X. S. Wang, R. Cao, *Chem. Soc. Rev.* **2017**, *46*, 126-157.

[6] a) M. Kandiah, M. H. Nilsen, S. Usseglio, S. Jakobsen, U. Olsbye, M. Tilset, C. Larabi, E. A. Quadrelli, F. Bonino, K. P. Lillerud, *Chem. Mat*. **2010**, *22*, 6632-6640; b) Y. Bai, Y. B. Dou, L. H. Xie, W. Rutledge, J. R. Li, H. C. Zhou, *Chem. Soc. Rev*. **2016**, *45*, 2327-2367; c) M. Rimoldi, A. J. Howarth, M. R. DeStefano, L. Lin, S. Goswami, P. Li, J. T. Hupp, O. K. Farha, *ACS Catal*. **2017**, *7*, 997-1014; d) D. Yang, B. C. Gates, *ACS Catal*. **2019**, *9*, 1779-1798.

[7] a) H. Wu, Y. S. Chua, V. Krungleviciute, M. Tyagi, P. Chen, T. Yildirim, W. Zhou, *J. Am. Chem. Soc*. **2013**, *135*, 10525-10532; b) G. C. Shearer, S. Chavan, J. Ethiraj, J. G. Vitillo, S. Svelle, U. Olsbye, C. Lamberti, S. Bordiga, K. P. Lillerud, *Chem. Mat.* **2014**, *26*, 4068-4071.

[8] M. Vandichel, J. Hajek, F. Vermoortele, M. Waroquier, D. E. De Vos, V. Van Speybroeck, *Crystengcomm* **2015**, *17*, 395-406.

[9] K. Xuan, Y. F. Pu, F. Li, A. X. Li, J. Luo, L. Li, F. Wang, N. Zhao, F. K. Xiao, *J. CO_2 Util*. **2018**, *27*, 272-282.

[10] R. J. Marshall, C. L. Hobday, C. F. Murphie, S. L. Griffin, C. A. Morrison, S. A. Moggach, R. S. Forgan, *J. Mater. Chem. A* **2016**, *4*, 6955-6963.

[11] X. Ma, L. Wang, Q. Zhang, H.-L. Jiang, *Angew. Chem. Int. Ed*. **2019**, *58*, 12175-12179.

[12] F. Vermoortele, B. Bueken, G. Le Bars, B. Van de Voorde, M. Vandichel, K. Houthoofd, A. Vimont, M. Daturi, M. Waroquier, V. Van Speybroeck, C. Kirschhock, D. E. De Vos, *J. Am. Chem. Soc.* **2013**, *135*, 11465-11468.

[13] Y. Liu, R. C. Klet, J. T. Hupp, O. Farha, *Chem. Commun.* **2016**, *52*, 7806-7809.

[14] a) J. C. Jiang, O. M. Yaghi, *Chem. Rev.* **2015**, *115*, 6966-6997; b) D. Yang, V. Bernales, T. Islamoglu, O. K. Farha, J. T. Hupp, C. J. Cramer, L. Gagliardi, B. C. Gates, *J. Am. Chem. Soc.* **2016**, *138*, 15189-15196.

[15] R. C. Klet, Y. Liu, T. C. Wang, J. T. Hupp, O. K. Farha, *J. Mater. Chem. A* **2016**, *4*, 1479-1485.

[16] D. Yang, M. A. Ortuno, V. Bernales, C. J. Cramer, L. Gagliardi, B. C. Gates, *J. Am. Chem. Soc.* **2018**, *140*, 3751-3759.

[17] R. Wei, C. A. Gaggioli, G. Li, T. Islamoglu, Z. Zhang, P. Yu, O. K. Farha, C. J. Cramer, L. Gagliardi, D. Yang, B. C. Gates, *Chem. Mat*. **2019**, *31*, 1655-1663.

[18] M. J. Katz, Z. J. Brown, Y. J. Colon, P. W. Siu, K. A. Scheidt, R. Q. Snurr, J. T. Hupp, O. K. Farha, *Chem. Commun.* **2013**, *49*, 9449-9451.

[19] Z. L. Fang, B. Bueken, D. E. De Vos, R. A. Fischer, *Angew. Chem. Int. Ed.* **2015**, *54*, 7234-7254.

[20] G. Cai, H. L. Jiang, *Angew. Chem. Int. Ed.* **2017**, *56*, 563-567.

[21] a) J. H. Cavka, S. Jakobsen, U. Olsbye, N. Guillou, C. Lamberti, S. Bordiga, K. P. Lillerud, *J. Am. Chem. Soc.* **2008**, *130*, 13850-13851; b) D. Yang, S. O. Odoh, T. C. Wang, O. K. Farha, J. T. Hupp, C. J. Cramer, L. Gagliardi, B. C. Gates, *J. Am. Chem. Soc.* **2015**, *137*, 7391-7396.

[22] N. Planas, J. E. Mondloch, S. Tussupbayev, J. Borycz, L. Gagliardi, J. T. Hupp, O. K. Farha, C. J. Cramer, *J. Phys. Chem. Lett.* **2014**, *5*, 3716-3723.

10.1002/ejic.202000031

WILEY-VCH

FULL PAPER

Text for Table of Contents

Esterification of levulinic acid with ethanol was catalyzed by the cooperative effects between the Lewis acid sites offered by unsaturated Zr_6 nodes and Brønsted acid sites supplied by OH in defective UiO-66 MOFs with high defect density, which was tuned by precursor ratios and modulators.

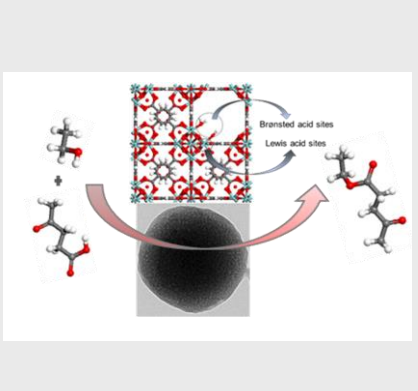

Key Topic for Table of Contents

UiO-66, Catalysis

*Author(s), Corresponding Author(s)**

Ruiping Wei, Jingdeng Fan, Xumin Qu, Lijing Gao, Yuanfeng Wu, Zhongqi Zhang, Feng Hu, Guomin Xiao*

Page No.1 – Page No.8

Title

Tuning the Catalytic Activity of UiO-66 via Modulated Synthesis : Esterification of Levulinic Acid as A Test Reaction